Journal of Materials Processing Tech. 250 (2017) 9–15

Contents lists available at ScienceDirect

Journal of Materials Processing Tech.

journal homepage: www.elsevier.com/locate/jmatprotec

Dynamics of solid-liquid interface and porosity formation determined through x-ray phase-contrast in laser welding of pure Al

Masanori Miyagi[a,*], Yousuke Kawahito[b], Hiroshi Kawakami[c], Takahisa Shoubu[d]

[a] Research & Development Group, Hitachi, Ltd. 7-1-1 Omika, Hitachi, Ibaraki 319 – 1292, Japan
[b] Osaka University, Joining and Welding Research Institute 11-1 Mihogaoka, Ibaraki, Osaka 567 – 0047, Japan
[c] Mie University, Graduate School of Engineering 1577 Kurimamachiya-cho, Tsu, Mie 514 – 8507, Japan
[d] Japan Atomic Energy Agency, Sector of Nuclear Science Research Materials Sciences Research Center, 1-1-1 Kouto, Sayo-cho, Sayo-gun, Hyogo 679–5148, Japan

ARTICLE INFO

Keywords:
Laser welding
Pure Al
Keyhole
X-ray phase contrast

ABSTRACT

Through X-ray phase contrast method, solid-liquid interface, keyhole, and porosity in laser welding of pure Al could be clearly observed, and the shapes could be quantitatively evaluated. Almost no molten metal occurred at the keyhole bottom, and the temperature gradient and cooling rate there were estimated to be enormously large as compared to other locations in the weld pool. The flow of molten metal around the keyhole bottom was about twice as fast as in the upper part of the weld pool, suggesting that the amount of heat transport around the bottom was larger than in the upper part. Porosity formation is determined by keyhole behavior. In the case of a stable keyhole, obtained with a fan to remove the laser-induced plume, the porosity rate was around 6%, and the gas in the voids consisted entirely of hydrogen. In the case of an unstable keyhole, obtained without fan usage, the porosity rate was around 18%, and the gas included a component of air (nitrogen) in addition to hydrogen.

1. Introduction

In laser welding, a high power density can easily be obtained to achieve deeper penetration with a higher weld speed than in arc welding. In addition, highly accurate laser welding can be achieved with a small spot size, e.g., 0.1 mm, because of recent technological innovations related to laser sources and optics. Laser welding phenomena and defect formation mechanisms, however, are still not properly understood because of the highly complicated process of mixing solid, liquid, gas, and plasma phases. It is difficult to control the laser welding process precisely in some cases. Thus, a method of process control based on an in-depth understanding of laser welding phenomena and mechanisms has long been sought. It is difficult, however, to control weld quality with aluminum because it exhibits high reflectivity of 1-μm laser light, in addition to having higher thermal conductivity than that of conventional steel. Therefore, to suppress defects in laser welding of aluminum, it is important to understand the welding phenomena in detail.

Defects in laser welding include porosity, which is the appearance of pores in the weld metal; under-fill, which is dents on the welding surface; spatter, which is small pieces of weld metal flying out of the weld pool; and cracks in the weld metal and heat-affected zones. For these weld defects, analysis by X-ray imaging technology has been performed since around 2000. For laser welding of stainless steel, Kawahito et al. (2015) applied X-ray image analysis of the keyhole and melt pool to demonstrate that part of the melt flow accelerating along the upward convection behind the keyhole results in spattering. For laser welding of copper, Heider et al. (2013) showed that keyhole expansion results in spattering, as part of the melt pool is ejected by the increased pressure inside the keyhole. Miyagi and Zhang (2015) used high-speed X-ray imaging to observe the weld pool dynamics for laser welding of pure copper under several welding conditions and found the same mechanism of melt pool ejection reported by Heider et al. (2013). Regarding investigation of the porosity formation mechanism by X-ray imaging analysis, we know from reports by Matsunawa et al. (2003) and Katayama and Matsunawa (2002) that keyhole instability due to localized evaporation at the keyhole wall leads to porosity. By applying in-situ X-ray observation, Kawahito et al. (2009) reported that in laser welding of stainless steel with a 10-kW fiber laser, bubbles in the melt pool leading to pores were formed not only at the bottom of the keyhole but also in the upper or middle parts of the weld pool.

Although in-situ observation with X-rays is useful for understanding laser welding phenomena, images obtained by the X-ray absorption method have limited clarity: the solid-liquid interface and keyhole shape are difficult to distinguish clearly because of the low density differences. As a result, the mechanism for the elementary step of laser

* Corresponding author.
E-mail address: masanori.miyagi.dc@hitachi.com (M. Miyagi).

http://dx.doi.org/10.1016/j.jmatprotec.2017.06.033
Received 18 March 2017; Received in revised form 17 June 2017; Accepted 19 June 2017
Available online 27 June 2017

Table 1
Chemical composition of A1050 (mass%).

Material	Al	Si	Fe	Cu	Mn	Mg	Cr	Zn	Ti	V
A1050	99.6	0.1	0.29	0	0	0	–	0	0.03	0.01

welding remains unclear. New observation technologies are thus necessary for deep understanding of laser welding phenomena. Therefore, in this research, we investigated the laser welding phenomena of aluminum by applying an X-ray phase contrast method as an imaging technique. It is a method of converting the phase change occurring when X-ray pass through an object into contrast and producing image.

2. Experimental procedure

Pure aluminum A1050 was used in the experiments because it readily exhibits weld defects such as porosity. We used a pure Al plate with dimensions of 70 × 30 × 3 mm. Table 1 lists the chemical composition of A1050. For investigating the welding phenomena of A1050, a single-mode fiber laser with a maximum output power of 500 W was used. The laser beam was focused on the weld point by a lens with a focal length of 190 mm. Fig. 1 shows the laser beam profile at a −1 mm defocus distance, which confirmed that a low-beam-intensity area occurred at the outer circumference. The spot size at the −1 mm defocus distance was around 140 μm. This special laser beam condition was selected because of a limitation of the chosen X-ray phase contrast method, in which the observation area for the SPring-8 (Super Photon ring–8 GeV) X-ray source of was 1 × 1 mm. A proper weld pool size could be obtained with this laser beam condition. To avoid reflection off the A1050 sample, the laser beam irradiated it at a 10° angle.

Fig. 2 illustrates the principles of X-ray absorption contrast and X-ray phase contrast. When an X-ray transmits to a target, its phase changes and interference occurs. In the X-ray phase contrast method, an image is obtained from a contrasting stripe pattern based on the differences in refractive index among the gas, liquid, and solid phases. The resulting image therefore shows a clearer outline of the target than that obtained by X-ray absorption contrast. Because the X-ray phase contrast method requires a highly coherent, monochromatic X-ray, we used the X-ray of the undulator beam line (BL22XU) at SPring-8 for this experiment. SPring-8 is a large synchrotron radiation facility which delivers the most powerful synchrotron radiation currently available.

Fig. 3 shows our laser welding and in-situ observation system setup using the X-ray phase contrast method. The sample was arranged vertically and then penetrated horizontally by X-ray radiation. For welding, the laser beam irradiated the sample from the top and impacted the material on its narrow edge. The keyhole and weld pool were visualized with the X-rays, and an image was captured by a high-speed video camera at a frame rate of 1 kHz.

The joint configuration was bead-on-plate, and the welding length was 30 mm. In this study, the laser power, weld speed and defocus distance were fixed at 500 W, 1 m/min, and −1 mm, respectively. The welding tests were conducted both with and without using a fan to remove a laser-induced plume. To investigate porosity, the gas composition and quantity were analyzed with a quadrupole mass spectrometer. The locations of voids were identified by X-ray imaging, and gas samples were then obtained by drilling in vacuum.

3. Results and discussion

3.1. Laser welding phenomena: quantitative evaluation of keyhole and weld pool geometry

Fig. 4 shows an X-ray phase contrast image and schematic of the keyhole and weld pool at a certain time during laser welding with a fan in use. Since the shape of the weld pool could be clearly observed, the weld pool shape and measurement results are shown in the schematic. The penetration depth was 0.58 mm, and the keyhole width was 0.040 mm. The diameter of the bubble in the weld pool was 0.025 mm. The distance from the keyhole to the back of the weld pool was 0.38 mm, and the distance from the bottom of the keyhole to the solid-liquid interface was 9.0×10^{-3} mm. Further, the growth direction of the solid-liquid interface at point Y shows an inclination of 34.0° from the horizontal direction.

Since the gas-liquid and solid-liquid interfaces could be clearly observed, we estimated the thermal characteristics of the weld pool. Table 2 lists the physical property values used for estimating the thermal characteristics, and Table 3 lists the calculation results. From the weld speed and the shape of the weld pool, the growth rate, cooling rate, and temperature gradient of the weld pool were estimated. As for the temperature gradient, since the gas-liquid interface and the solid-liquid interface can be observed, the liquid phase distance was measured and temperature gradient was calculated. The cooling rate between the gas-liquid interface and the solid-liquid interface was determined using the time until solidification. The growth rate was calculated by measuring the angle between the direction of the weld line and the growth direction. With increasing measurement depth, a lower growth rate but a larger cooling rate and temperature gradient were obtained. At point X, since the surface of the weld pool was in

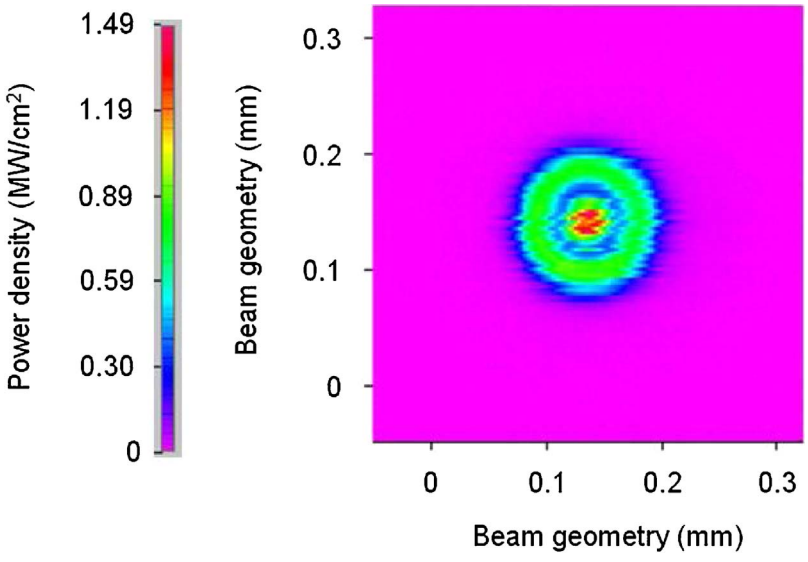

Fig. 1. Laser beam intensity profile (defocus distance = −1 mm).